Using dark states for exciton storage in transition-metal dichalcogenides

2016 J. Phys.: Condens. Matter 28 034005

(http://iopscience.iop.org/0953-8984/28/3/034005)

IOP Publishing Journal of Physics: Condensed Matter
J. Phys.: Condens. Matter **28** (2016) 034005 (6pp) doi:10.1088/0953-8984/28/3/034005

Using dark states for exciton storage in transition-metal dichalcogenides

Frank Tseng[1,2], Ergun Simsek[3] and Daniel Gunlycke[2]

[1] National Research Council Research Associate, Washington DC 20001, USA
[2] Naval Research Laboratory, Washington DC 20375, USA
[3] The George Washington University, Washington DC 20052, USA

E-mail: daniel.gunlycke@nrl.navy.mil

Received 5 May 2015
Accepted for publication 16 September 2015
Published 24 December 2015

Abstract

We explore the possibility of storing excitons in excitonic dark states in monolayer semiconducting transition-metal dichalcogenides. In addition to being optically inactive, these dark states require the electron and hole to be spatially separated, thus inhibiting electron/hole recombination and allowing exciton lifetimes to be extended. Based on an atomistic exciton model, we derive transition matrix elements and an approximate selection rule showing that excitons could be transitioned into and out of dark states using a pulsed infrared laser. For illustration, we also present exciton population scenarios based on a population analysis for different recombination decay constants. Longer exciton lifetimes could make these materials candidates for applications in energy management and quantum information processing.

Keywords: transition-metal dichalcogenides, dark exciton states, exciton storage

(Some figures may appear in colour only in the online journal)

1. Introduction

An exciton can be formed when an electron excited across a semiconducting crystal band gap and the corresponding hole left behind mutually experience an attractive Coulomb interaction. Among host materials for excitons, monolayer transition-metal dichalcogenides are of particular interest for a number of reasons. For one, these excitons are restricted to two dimensions (2D). These materials also exhibit a direct band gap [1–3] and experiments suggest that exciton binding energies could be as large as 0.3–1 eV [4–10], which is one to two orders of magnitude higher than in typical semiconductors. While single photons can be absorbed to generate optically bright excitons, these excitons are also subject to spontaneous electron/hole recombination, releasing the photons back to the environment. Furthermore, exciton lifetimes in the transition-metal dichalcogenides at room temperature have yet to reach 1 ns [11, 12]. Delaying the recombination process could have impact in quantum computing, quantum information processing, and energy storage applications [13–16], and potentially even enable Bose–Einstein condensation of excitons [17].

We propose herein the use of excitonic dark states to extend exciton lifetimes in the transition-metal dichalcogenides. Dark states are optically inactive and therefore often ignored. Their presence, however, have been detected in many low-dimensional structures, including quantum-dots [16, 18, 19], quantum-wells [20–23], and carbon-nanotubes [24–26]. Recently, two-photon experiments also revealed dark exciton states in monolayer tungsten disulphide (WS_2) [8], a member of the transition-metal dichalcogenide family. Unlike bright exciton states, the symmetry in these dark states requires that the electron and hole are spatially separated, which inhibits radiative recombination [18]. The scattering rate between bright and dark states depends on the energy separation between these states. To limit spontaneous scattering, it is therefore beneficial to work with a material, in which the subshell degeneracy predicted in the hydrogen model [27–29] for excitons is lifted. The transition-metal dichalcogenides are again particularly promising, as lattice effects separate the dark $2p$ and the bright $2s$ states by an energy [8, 30] larger than kT at room temperature. See the schematic diagram of the lowest exciton levels in figure 1(a). Note that this diagram also contains two $1s$ levels, usually referred to as 'A' and 'B' [4, 31]. The latter excitons originate from a spin-split valence band due to the spin-orbit interaction [4, 31, 32]. Using a laser to excite electrons across the band gap, we could generate an

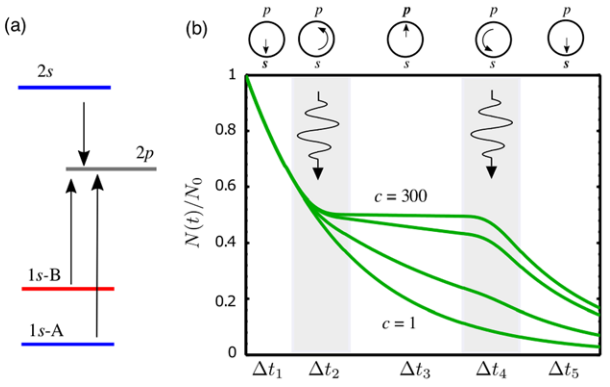

Figure 1. (a) Schematic exciton energy diagram for transition-metal dichalcogenides, illustrating considered transitions from bright states (blue and red) to a dark $2p$ state (grey). (b) The decay of the total exciton population is slower when the excitons populate the dark $2p$ state. Four scenarios are presented assuming a bright/dark decay constant ratio c of 1, 2, 20, and 300.

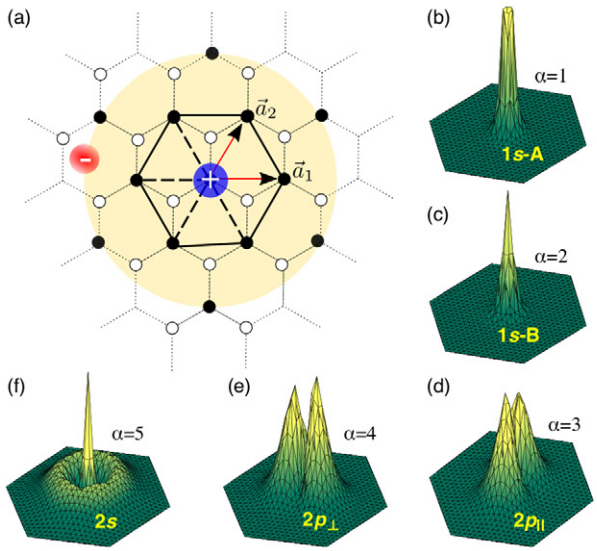

Figure 2. (a) Schematic illustration of an exciton residing on the triangular-tiled lattice structure formed by the black transition-metal sites. (b)–(f) Probability density $|\xi_\alpha(\vec{R})|^2$ of the exciton eigenfunctions $\xi_\alpha(\vec{R})$ obtained from the 3-ALE model with quantum numbers α and corresponding 2D-H model labels. The eigenfunctions are sorted in order of increasing energy.

exciton population in chosen bright s-states. A second laser tuned to resonance with the desired exciton transition would then controllably move that population into the $2p$ states. As illustrated in figure 1(b), the second laser could also be used to return the population to the s-states at a later point. This ability to control the release of the stored excitation energy could have application in energy management.

Section 2 presents the theoretical approach for calculating the exciton population and the needed transition matrix elements. The transition matrix elements involve exciton states, which we obtain from an atomistic exciton model referred to as the triangular lattice exciton (3-ALE) model [30]. Section 3 presents and discusses numerical results and makes comparison to corresponding results derived from the 2D hydrogen (2D-H) model. Section 4 is a summary with conclusions.

2. Theoretical approach

2.1. Formulation

Consider a photo-induced zone-centre exciton in a state $|\xi_\alpha\rangle$ with the quantum number α describing the relative motion of the electron and hole. As there are no spin scattering processes herein, we have for brevity dropped the spin quantum number from our notation. For strongly bound excitons, we can label the quantum number α using the corresponding quantum numbers of the 2D-H model with an extra 'A' or 'B' for the case of $1s$. We focus below on $1s$-A, $1s$-B, $2s$, and $2p$ and note that, unlike the s-states, there are two $2p$ states for each spin (see figure 2).

Using the second laser mentioned above, we can couple the state $|\xi_\alpha\rangle$ to a second state $|\xi_{\alpha'}\rangle$. This coupling is modelled through the electric field $\vec{E}$ generated from the electromagnetic radiation, which we assume to be a plane wave with an angle of incidence normal to the plane of the monolayer transition-metal dichalcogenides. Assuming that the two $2p$ states are practically degenerate, the exciton population could be moved into either state. As there is no discrimination, we could assume any laser polarisation. For demonstration, we choose linear polarisation along an arbitrary in-plane direction $\hat{\rho}$. The electric field on the monolayer surface can then be expressed as $\vec{E} = |\vec{E}|\hat{\rho}\cos\omega t$, where ω is the laser frequency and t is time. This field can be described by the electric potential, which satisfies $\vec{E} = -\nabla\phi$. Ignoring the unimportant constant, this potential is

$$\phi(\rho, t) = \phi(\rho)\cos\omega t, \tag{1}$$

where the spatial factor is given by $\phi(\rho) = -|\vec{E}|\rho$.

2.2. Transition matrix elements

We expand the exciton states in a minimal orthonormal lattice basis, which gives

$$|\xi_\alpha\rangle = \sum_{\vec{R}} \xi_\alpha(\vec{R})|\vec{R}\rangle, \tag{2}$$

where $\vec{R}$ are lattice vectors. With the electron charge being $-e$, we could express the transition matrix elements as

$$\begin{aligned}\Gamma_{\alpha'\alpha} &= -e\langle\xi_{\alpha'}|\phi(\rho)|\xi_\alpha\rangle \\ &= e|\vec{E}|\hat{\rho}\cdot\sum_{\vec{R}}\vec{R}\,\xi^*_{\alpha'}(\vec{R})\,\xi_\alpha(\vec{R}).\end{aligned} \tag{3}$$

Let us now derive an approximate selection rule based on a D_{6h} pseudo-symmetry present in the monolayer transition-metal dichalcogenides [30]. One symmetry element of this pseudo-symmetry is inversion. The exciton eigenfunction $\xi_\alpha(\vec{R})$ is therefore an approximate eigenfunction of the parity operator $\mathcal{P}$ so that

$$\mathcal{P}\xi_\alpha(\vec{R}) \approx s_\alpha\xi_\alpha(\vec{R}), \tag{4}$$

where the eigenvalues are given by

$$s_\alpha = \begin{cases} +1 & (s \text{ states}), \\ -1 & (p \text{ states}). \end{cases} \tag{5}$$

Using the parity relation above, we can rewrite the transition matrix elements as

$$\Gamma_{\alpha'\alpha} \approx e|\vec{E}|\hat{\rho} \cdot \sum_{\vec{R}} \vec{R}\, \xi^*_{\alpha'}(\vec{R})\, \xi_\alpha(\vec{R}) \frac{1 - s_{\alpha'} s_\alpha}{2}. \tag{6}$$

This is an approximate form of Laporte's rule [33] and shows that transition matrix elements between two bright states or two dark states should be quite small. The focus below, however, is on transitions between bright s-states and dark p-states.

Considering the direct-space representation of the nearly degenerate $2p$ states, we denote these orthogonal states as $2p_\parallel$ and $2p_\perp$, as shown in figures 2(d) and (e), respectively, with the indices referring to their direction relative to the polarisation vector $\hat{\rho}$. Ignoring perturbations from the lattice, we find from reflection symmetry that the electric field only couples s-states to the $2p_\parallel$ state, thus when we refer to transitions to $2p$, we mean transitions to $2p_\parallel$, to be exact.

2.3. Exciton population analysis

When the charged carriers interact with a time-varying electric-field, its population oscillates sinusoidally [34] between states of opposite parity. Assuming that an exciton is in a state $|\xi_\alpha\rangle$ at $t = 0$, the probability of finding it in the state $|\xi_{\alpha'}\rangle$ at a later time t is

$$P_{\alpha'\alpha}(t) = \frac{|\Gamma_{\alpha'\alpha}|^2}{|\Gamma_{\alpha'\alpha}|^2 + \hbar^2(\omega - \omega_{\alpha'\alpha})^2/4} \sin^2 \Omega_{\alpha'\alpha}\, t, \tag{7}$$

where $\Omega_{\alpha'\alpha} \equiv \sqrt{|\Gamma_{\alpha'\alpha}|^2/\hbar^2 + (\omega - \omega_{\alpha'\alpha})^2/4}$ is the generalised Rabi frequency and $\omega_{\alpha'\alpha} \equiv \omega_{\alpha'} - \omega_\alpha$ is the energy separation of the states involved in the transition. To maximise the number of excitons being moved between the states, we assume that the laser frequency is on-resonance with $\omega = \omega_{\alpha'\alpha}$, which gives

$$P_{\alpha'\alpha}(t) = \sin^2 \frac{|\Gamma_{\alpha'\alpha}|t}{\hbar}. \tag{8}$$

A scenario of controlled excitations to and from one of the dark 2p states is illustrated in figure 1, which shows possible progressions of the total exciton population $N(t)$ as function of time. In the first time interval Δt_1, the generated exciton population $N(0) = N_0$ decays from an s-state described by the rate equation $\mathrm{d}N/\mathrm{d}t = -\lambda_s N$, where λ_s represents the decay constant of that state. In the time interval Δt_2, the second on-resonant laser excites the remaining population for storage in a dark $2p$-state. The rate equation

$$\frac{\mathrm{d}N}{\mathrm{d}t} = -\lambda_s N_1 \cos^2 \frac{|\Gamma_{\alpha'\alpha}|t_1}{\hbar} - \lambda_p N_1 \sin^2 \frac{|\Gamma_{\alpha'\alpha}|t_1}{\hbar}, \tag{9}$$

where $N_1 = N(\Delta t_1)$, $t_1 = t - \Delta t_1$, and λ_p is the decay constant of the dark $2p$ state describes the storage process. At the onset of Δt_3, the laser is turned off to keep the exciton in the $2p$ state with the decay rate $\mathrm{d}N/\mathrm{d}t = -\lambda_p N$. To compare the evolution of the exciton population with and without the use of the dark $2p$ state, it is useful to define the decay constant ratio $c \equiv \lambda_s/\lambda_p$. Because the $2p$ state is dark, we expect $c \gg 1$, which would allow excitons to be stored in the $2p$-state for a relatively long time.

To release the exciton population from the dark $2p$ state back to the s-state, we could again use the on-resonant laser pulse. The corresponding decay rate for the release process in the time interval Δt_4 is the same as in equation (9), except for swapping $\lambda_s \leftrightarrow \lambda_p$ and letting the time and population indices $1 \rightarrow 3$. After the population has returned to the s-state, the laser is switched off and the decay, during Δt_5, is once again described by the decay constant λ_s.

2.4. Triangular lattice exciton model

To characterise the two-dimensional excitons in the transition-metal dichalcogenides, we adopt a model referred to as the triangular lattice exciton model [30]. This model assumes an orthonormal basis $|\vec{R}\rangle$ centred on the transition-metal sites, shown in figure 2, which form the equilateral triangular lattice in the monolayer transition-metal dichalcogenides. Using this basis, we express the exciton Hamiltonian [30]

$$\begin{aligned} H = &\sum_{\vec{R}\vec{\delta}} T_{\vec{\delta}} |\vec{R} + \vec{\delta}\rangle\langle\vec{R}| + \sum_{\vec{R}} E_0 |\vec{R}\rangle\langle\vec{R}| \\ &- \sum_{\vec{R}\neq 0} V_{\vec{R}} |\vec{R}\rangle\langle\vec{R}| - V_0 |\vec{0}\rangle\langle\vec{0}|, \end{aligned} \tag{10}$$

where $\vec{\delta}$ are vectors to the nearest-neighbour sites, $T_{\vec{\delta}}$ are hopping elements, E_0 is a reference energy, and $V_{\vec{R}}$ and V_0 are Coulomb interaction elements. The nearest-neighbour vectors are $\vec{\delta} \in \{\pm\vec{a}_1, \pm\vec{a}_2, \pm(\vec{a}_1 - \vec{a}_2)\}$, where $\vec{a}_1 = a\hat{x}$ and $\vec{a}_2 = a\left(\hat{x} + \sqrt{3}\,\hat{y}\right)/2$ are the lattice vectors shown in figure 2 with a being the lattice constant. The hopping elements are

$$T_{\vec{\delta}} \equiv \frac{4\mathrm{Ry}}{3m}\left(\frac{a_0}{a}\right)^2 + \mathrm{i}\frac{\Delta E_{\mathrm{SO}}}{9} \sin \vec{K} \cdot \vec{\delta}, \tag{11}$$

where m is the reduced effective mass in units of the electron mass m_0, a_0 is the Bohr radius, ΔE_{SO} is the spin-orbit coupling, and $\vec{K} = 4\pi\hat{x}/3a$ is a wave vector at a Brillouin zone corner. The onsite energy

$$E_0 \equiv -\frac{4\,\mathrm{Ry}}{m}\left(\frac{a_0}{a}\right)^2 - \frac{\Delta E_{SO}}{2} \tag{12}$$

sets the reference energy for excitations between the band edges to zero. Lastly, the off-centre Coulomb potential is

$$V_{\vec{R}} = \frac{\mathrm{Ry}}{\varepsilon_r} \frac{2a_0}{|\vec{R}|}, \tag{13}$$

where ε_r is a dimensionless dielectric constant and $|\vec{R}|$ is the relative distance between the electron and the hole. To determine the shared-site potential V_0, we assume that the exciton binding energy from the 2D-H model describes weakly bound states that span several transition-metal lattice sites reasonably well. Therefore, we estimate V_0 by matching the binding energies of the $1s$-A state of the 3-ALE model and the $1s$ state of the 2D-H model, at the relatively large dielectric constant

Table 1. Material parameters used in the 3-ALE model.

	a [Å]	ΔE_{SO} [eV]	m [m_0]	V_0 [eV]
MoS_2	3.18	0.152	0.32	1.44
WS_2	3.19	0.425	0.25	1.67

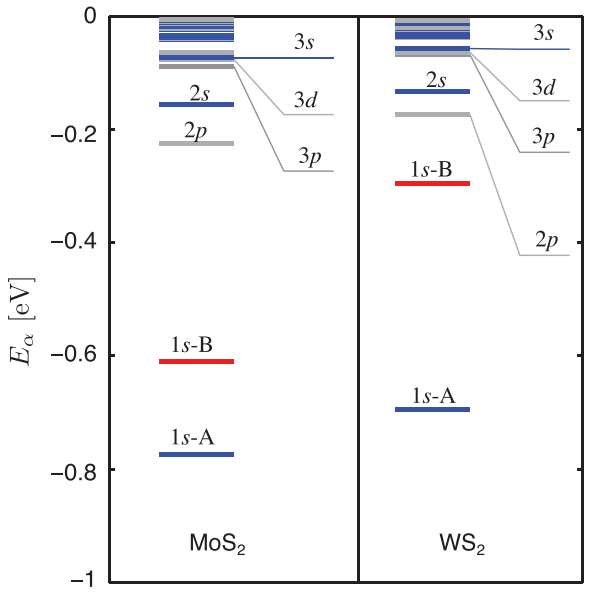

Figure 3. The discrete energy spectrum for zone-centre excitons in MoS_2 and WS_2, assuming the dielectric constant $\varepsilon_r = 3$. Blue and red lines are energy levels from bright exciton states originating from the valence and split-off bands, respectively. Grey lines are levels from dark states.

$\varepsilon_r = 10$. The shared-site potential V_0 and other material-dependent parameters used herein are listed in table 1.

The exciton states introduced in equation (2) are eigenstates of the Hamiltonian in equation (10) and thus solutions to

$$H|\xi_\alpha\rangle = E_\alpha|\xi_\alpha\rangle, \tag{14}$$

where E_α are the discrete energies of the bound exciton states.

3. Results and discussions

The probability densities $|\xi_\alpha(\vec{R})|^2$ in figure 2 describe the likelihood of finding the electron at site $\vec{R}$, assuming the hole centred at $\vec{R} = \vec{0}$. To lowest order, the probability of excitons being generated or recombined through single-photon events is proportional to the probability of finding the electron and hole in the same location. The oscillator strength $|\xi_\alpha(\vec{0})|^2$ is zero by symmetry for the dark $2p$ states (see figure 2). This implies that electrons and holes in dark exciton states cannot recombine. In practice, we expect some recombination due to coupling of s- and p-states by contaminants, disorder, and lattice vibrations.

Through improved fabrication processes, contaminants and disorder could hopefully be kept to a minimum. Lattice vibrations are usually thornier, as we have less control over coupling due to phonons. It is expected, however, that

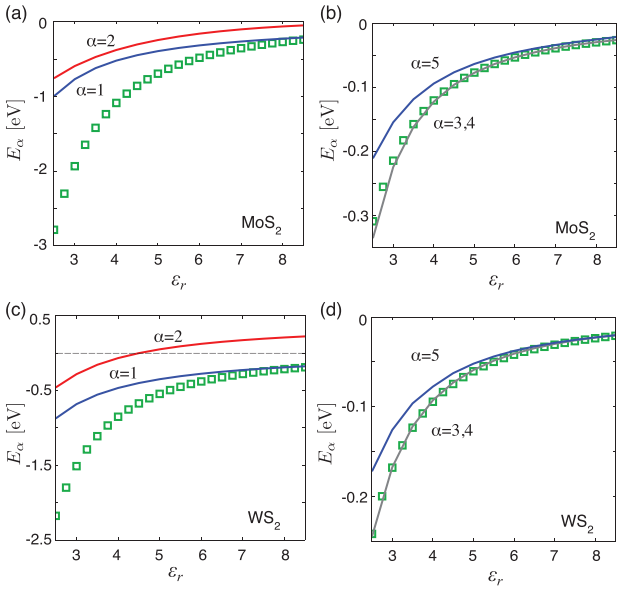

Figure 4. Binding energies of zone-centred excitons in MoS_2 and WS_2 as a function of the dielectric constant obtained from the 3-ALE model (solid curves) and the 2D-H model (squares). (a) The hydrogen model fails to describe the two $1s$ states unless ε_r is large. (b) The $2s$- and $2p$ states are well separated in energy for small ε_r. (c) The $1s$-B state is well separated from the $1s$-A state due to a large spin-orbit coupling and enters the energy continuum (above the dashed line) near $\varepsilon_r = 4$. (d) The hydrogen model is doing better for the $2p$ state as symmetry prohibits the electron and hole to occupy the same site.

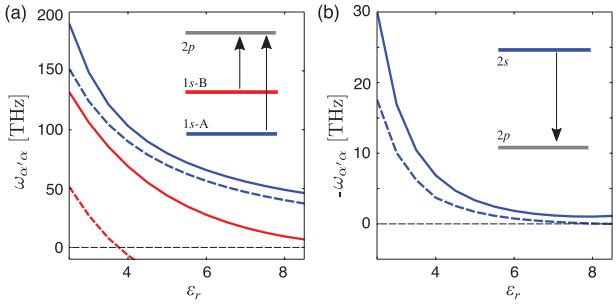

Figure 5. Frequencies as a function of the dielectric constant for transitions into a $2p$ state from (a) the $1s$ states and (b) the $2s$ state. Solid and dashed curves represent MoS_2 and WS_2, respectively.

scattering due to phonons is less effective if the dark states of interest are energetically separated from the bright states. The energy levels E_α shown in figure 3 indicates that the bright-dark-state energy separation, specifically between the $2s$ and $2p$ states, is approximately 42 meV and 70 meV for tungsten disulphide WS_2 and molybdenum disulphide MoS_2, respectively, assuming a dielectric constant of $\varepsilon_r = 3.0$. This is larger than the optical phonon energies in these materials [35], thus requiring multiple phonon scattering events to enable recombination. Therefore, decay rates in dark p-states has the potential to be orders of magnitude longer than in the bright s-states.

The significant energy separation between the $2s$ and $2p$ states follows from the weak dielectric screening in 2D semiconductors and concomitant lattice effects [30]. The weak screening allows the electrons and holes to be tightly bound on the atomic scale. This causes the 2D-H model to break down,

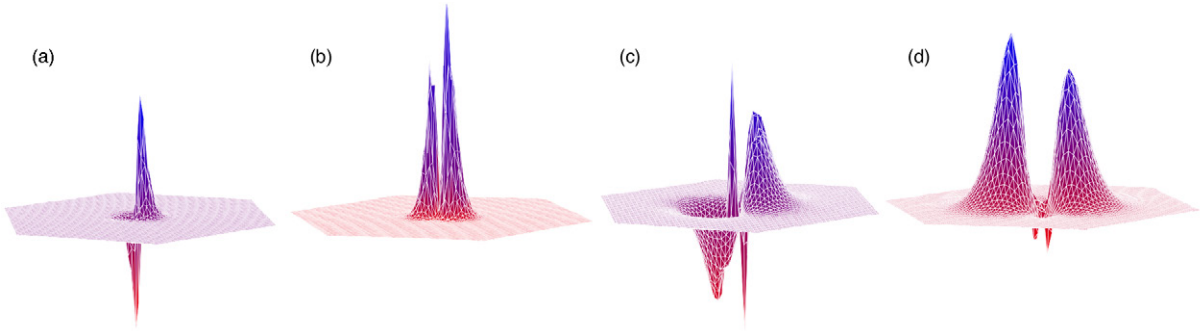

Figure 6. Transition matrix element contributions from different lattice sites in MoS_2 using a dielectric constant of 3.5. Transition from the 1*s*-A state when a uniform electric field in (a) absent and (b) present. (c) and (d) are the same as (a) and (b), respectively, except that the transition is from the 2*s* state. Because the positive and negative contributions cancel in (a) and (c), we could control the coupling between bright and dark states by switching on and off the electric field. Also note that the transition matrix element from 2*s* in (d) is larger than that from 1*s*-A in (b) due to the greater extent of the 2*s* exciton.

together with its predicted shell degeneracy. The energy separation is largest for the second shell and then becomes smaller for higher shells (see the energy levels of 3*s*, 3*p*, and 3*d* states in figure 3).

At the moment, there is no consensus on the interpretation of excitonic features [4, 6, 8, 10, 36–38]. This has created uncertainty as to where the electron/hole continuum is located. As this uncertainty extends to the dielectric constant, we present the energy levels as a function of the latter in figure 4. We have already assumed that the excitons are well described by the 2D-H model at large dielectric constants. For the small dielectric constant [9, 35, 39] expected for these materials, however, the results diverge as a result of the electron/hole separation approaching the lattice constant.

The breakdown of the predicted subshell degeneracy more importantly allows us to consider transitions into the dark 2*p* state from 1*s*-A, 1*s*-B, and 2*s*. Figure 5 shows the needed laser frequencies for these transitions. Depending on the dielectric constant, the frequencies should lie in the near- to mid-infrared regime for the first two transitions and mostly the far-infrared for the transition from 2*s*.

The on-resonant laser acts as an optical switch opening and closing exciton movement between bright and dark states. Figure 6 shows the direct space site contributions to the bright/dark transition matrix elements. When the second pulsed laser is in the off-state, there is no electric field and the electric potential is uniform. As the 1*s*-A exciton state is orthogonal to the 2*p* states, positive and negative contributions cancel, as shown in figure 6(a). If, on the other hand, the laser is in the on-state, we obtain a finite transition matrix element (see figure 6(b)). The same parity rule also applies to transitions from 1*s*-B and 2*s* shown in figures 6(c)and (d). Hence, we could controllably switch on and off the coupling between bright and dark exciton states.

The finite transition matrix elements $\Gamma_{\alpha'\alpha}$ has an approximate linear relationship with respect to the dielectric constant, as can been seen in figure 7. To understand this relationship, we note that a stronger dielectric screening leads to a greater spatial extent of the exciton wave functions, which in turn increases the sum over the direct space contributions. This is apparent in the 2D-H model, from which we have derived

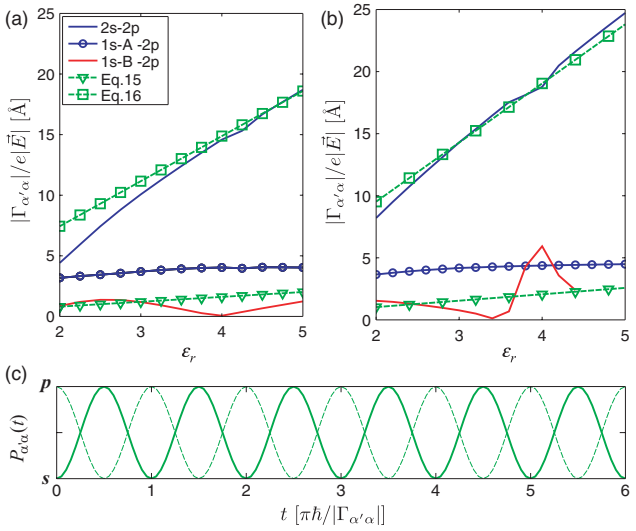

Figure 7. The magnitude of the considered transition matrix elements as a function of the dielectric constant for (a) MoS_2 and (b) WS_2. (c) The probability of finding an exciton in the bright *s* and dark *p* states oscillates as function of time. The solid and dashed curves represent population and depopulation, respectively, of the dark 2*p* state.

$$|\Gamma_{1s,2p_\parallel}| = \frac{\sqrt{3}}{16}\frac{9\,a_0\,\varepsilon_r}{4m}e|\vec{E}|, \tag{15}$$

and

$$|\Gamma_{2s,2p_\parallel}| = \frac{9\,a_0\,\varepsilon_r}{4m}e|\vec{E}|, \tag{16}$$

for the transitions from the 1*s* and 2*s* states, respectively. For comparison, these expressions are also shown in figure 7. The anomalous peak in the transition from 1*s*-B in WS_2 is presumably a result of the 1*s*-B and 2*p* energy levels crossing near $\varepsilon_r \approx 3.7$ (see figure 5). We also find that the coupling to the dark 2*p* state is stronger from the 1*s*-A state than the 1*s*-B state.

The magnitude of the two-state exciton coupling affects the dynamics of the exciton population. At resonance, the exciton population is subject to Rabi oscillations, which has a period

$T = \pi\hbar/|\Gamma_{\alpha'\alpha}|$. As shown in figure 1(b), we want the laser pulse to end when the exciton population has completely transitioned to the final state. Therefore, the desired pulse length of the second laser (see Δt_2 and Δt_4 in figure 1) needs to be odd integer multiples of $\pi\hbar/|2\Gamma_{\alpha'\alpha}|$. To minimise the needed laser pulse duration we assume $\Delta t_2 = \Delta t_4 = T/2 = \pi\hbar/2|\Gamma_{\alpha'\alpha}|$. One might also consider using a relatively high laser intensity, as the transition coupling is directly proportional to the electric field amplitude.

4. Conclusions

Dark exciton states could be exploited to extend exciton lifetimes in monolayer transition-metal dichalcogenides. The approximate selection rules derived herein show that these dark states could be accessed using a pulsed laser. Using an atomistic lattice model, we have estimated the needed frequency to be in the far-infrared to near-infrared range, depending on the chosen transition. Pulse durations are obtained from the Rabi frequency, which is inversely proportional to the transition matrix elements. These transition matrix elements have been computed using the atomistic lattice model and depend on the dielectric environment and material parameters as well as the pulsed laser intensity. Extending exciton lifetimes using dark exciton states could lead to future applications from energy storage to quantum information processing and might even make feasible Bose-Einstein condensation for excitons.

Acknowledgments

This work has been funded by the Office of Naval Research (ONR), directly and through the Naval Research Laboratory (NRL). ES and FT acknowledge support from NRL through the ONR Summer Faculty Program and the NRC Research Associateship Program, respectively.

References

[1] Splendiani A, Sun L, Zhang Y, Li T, Kim J, Chim C Y, Galli G and Wang F 2010 *Nano Lett.* **10** 1271–5
[2] Mak K F, Lee C, Hone J, Shan J and Heinz T F 2010 *Phys. Rev. Lett.* **105** 136805
[3] Zhao W, Ghorannevis Z, Chu L, Toh M, Kloc C, Tan P H and Eda G 2013 *ACS Nano.* **7** 791–7
[4] Frindt R F and Yoffe A D 1963 *Proc. R. Soc.* A **273** 69–83
[5] Klots A R *et al* 2014 *Sci. Rep.* **4** 6608
[6] Chernikov A, Berkelbach T C, Hill H M, Rigosi A, Li Y, Aslan O B, Reichman D R, Hybertsen M S and Heinz T F 2014 *Phys. Rev. Lett.* **113** 076802
[7] Ugeda M M *et al* 2014 *Nat. Mater.* **13** 1091–5
[8] Ye Z, Cao T, O'Brien K, Zhu H, Yin X, Wang Y, Louie S G and Zhang X 2014 *Nature* **513** 214–8
[9] Lin Y X, Ling X, Yu L, Huang S X, Hsu A L, Lee Y H, Kong J, Dresselhaus M S and Palacios T 2014 *Nano Lett.* **14** 5569–76
[10] Hanbicki A T, Currie M, Kioseoglou G, Friedman A L and Jonker B T 2015 *Solid State Commun.* **203** 16–20
[11] Korn T, Heydrich S, Hirmer M, Schmutzler J and Schüller C 2011 *Appl. Phys. Lett.* **99** 102109
[12] Yuan L and Huang L 2015 *Nanoscale* **7** 7402–8
[13] Chen G, Bonadeo N H, Steel D G, Gammon D, Katzer D S, Park D and Sham L J 2000 *Science* **289** 1906–9
[14] Biolatti E, Iotti R C, Zanardi P and Ross F 2000 *Phys. Rev. Lett.* **85** 5647–50
[15] Krenner H J, Stufler S, Sabathil M, Clark E C, Ester P, Bichler M, Abstreiter G, Finley J J and Zrenner A 2005 *New J. Phys.* **7** 184
[16] Poem E, Kodriano Y, Tradonsky C, Lindner N H, Gerardot B D, Petroff P M and Gershoni D 2010 *Nat. Phys.* **6** 993–7
[17] Blatt J M, Böer K W and Brandt W 1962 *Phys. Rev.* **126** 1691
[18] Johansen J, Julsgaard B, Stobbe S, Hvam H M and Lodahl P 2010 *Phys. Rev.* B **81** 081304
[19] Meulenberg R W, Lee J R I, Wolcott A, Zhang J Z, Terminello L J and Buuren T V 2009 *ACS Nano.* **3** 325–30
[20] Cerne J, Kono J, Sherwin M S, Sundaram M, Gossard A C and Bauer G E W 1996 *Phys. Rev. Lett.* **77** 1131–4
[21] Carter S, Birkedal V, Wang C S, Coldren L A, Maslov A V, Citrin D S and Sherwin M S 2005 *Science* **310** 651–3
[22] Wagner M, Schneider H, Stehr D, Winnerl S, Andrews A M, Schartner S, Strasser G and Helm M 2010 *Phys. Rev. Lett.* **105** 167401
[23] Rice W D *et al* 2013 *Phys. Rev. Lett.* **110** 137404
[24] Maultzsch J, Pomraenke R, Reich S, Chang E, Prezzi D, Ruini A, Molinari E, Strano M S, Thomsen C and Lienau C 2005 *Phys. Rev.* B **72** 241402
[25] Srivastava A, Htoon H, Klimov V I and Kono J 2008 *Phys. Rev. Lett.* **101** 087402
[26] Shaver J, Kono J, Portugall O, Krstić V, Rikken G L J A, Miyauchi Y, Maruyama S and Perebeinos V 2007 *Nano. Lett.* **7** 1851–5
[27] Wannier G 1937 *Phys. Rev.* **52** 191
[28] Ralph H I 1965 *Solid State Commun.* **3** 303–6
[29] Shinada M and Sugano S 1966 *J. Phys. Soc. Japan* **21** 1936
[30] Gunlycke D and Tseng F 2015 arXiv:1504.04040v1
[31] Wilson J A and Yoffe A D 1969 *Adv. Phys.* **18** 193
[32] Bromley R A, Murray R B and Yoffe A D 1972 *J. Phys. C: Solid State Phys.* **5** 759
[33] Laporte O 1924 *Z. Phys.* **23** 135–75
[34] Rabi I I 1937 *Phys. Rev.* **51** 652–4
[35] Molina-Sánchez A and Wirtz L 2011 *Phys. Rev.* B **84** 155413
[36] Beal A and Liang W 1976 *J. Phys.* C **9** 2459
[37] He K, Kumar N, Zhao L, Wang Z, Mak K F, Zhao H and Shan J 2014 *Phys. Rev. Lett.* **113** 026803
[38] Zhu B, Chen X and Cui X 2015 *Sci. Rep.* **5** 9218
[39] Cheiwchanchamnangij T and Lambrecht W R L 2012 *Phys. Rev.* B **85** 205302